(*2*), and derived alvarezsaurids. Unlike most troodontids and microraptorines, but similar to *Archaeopteryx* and derived dromaeosaurids, the foot of *Mahakala* exhibits the plesiomorphic unconstricted condition for metatarsal III, further indicating that this avian trait may be the primitive condition for paravians. The distal end of metatarsal II is composed of an asymmetrical ginglymoid articular surface and phalanx II-2 has a well-developed proximal heel and hypertrophied ginglymoid trochlea. This suite of characters is present only in dromaeosaurids.

Phylogenetic analysis identifies *Mahakala* as a basal dromaeosaurid and supports paravian monophyly with birds (Avialae) as the sister group to a monophyletic Deinonychosauria (Dromaeosauridae + Troodontidae) (Fig. 3 and fig. S1). Although discovered in relatively young Cretaceous deposits, the basal position of *Mahakala* has several implications regarding our understanding of the early history of deinonychosaurians (*17*). First, *Shanag* from the Early Cretaceous of Mongolia (*18*) nests within the purported Gondwanan lineage of dromaeosaurids, Unenlagiinae. This topology complicates recently proposed vicariance-driven origin hypotheses for these groups (*4*, *19*). Second, these dinosaurs are united with Jehol microraptorines (*Microraptor*, *Graciliraptor*, and *Sinornithosaurus*) to form the sister group to derived dromaeosaurids from Laurasia (velociraptorines and allied forms). Third, the purported avialan *Jinfengopteryx* (*20*) is a troodontid. *Jinfengopteryx* has feathers; it thus demonstrates the presence of feathers of modern aspect in a troodontid.

Decrease in body size is a trend in coelurosaurs (*3*, *8*, *21*) and is thought to have played an important role in the origin of birds and flight (*6*, *11*, *22*–*24*). Dromaeosaurids and other coelurosaurs, however, may have undergone clade-specific increases in body size (*8*, *25*). Testing these trends requires empirical size reconstructions for each node of the coelurosaur tree. We estimated ancestral body sizes for each internal node (ancestral node) using body mass estimates from femoral length measurements. These data were treated as a continuous additive trait and optimized across the phylogeny (*16*).

Our analysis (fig. S2) indicates that small body size was not a derived condition at *Archaeopteryx* or Avialae, where flight evolution in theropods is currently inferred. The ancestral dromaeosaurid, troodontid, and deinonychosaurian are reconstructed as small, each with a body mass around 700 g (Fig. 3). The basal members of these lineages are the same size as the early avialan *Jeholornis*. Additionally, our results indicate that deinonychosaurs underwent four parallel trends of body size increase. Three of these events occurred within Dromaeosauridae: *Deinonychus* increased in size by more than two orders of magnitude, as did *Unenlagia,* and the *Achillobator* + *Utahraptor* clade increased by three orders of magnitude. A single trend of body size increase was observed in troodontid body size. These events were contemporaneous with a decrease in avialan body sizes. Our analysis implies that the ancestral paravian had a body size of 600 to 700 g and was ~65 cm long, roughly the size of the largest specimens of *Archaeopteryx* or *Sapeornis* and entailing the size range reconstructed for basal deinonychosaurs. Thus, miniaturization preceded the avialan node and the origin of flight, and as a result, hypotheses relating ontogenetic or metabolic controls on miniaturization to flight origin in theropods must be equally capable of explaining the size reduction within ancestral paravians and the iterative trends of size increase in deinonychosaurs.

References and Notes

1. J. Gauthier, *Mem. Calif. Acad. Sci.* **8**, 1 (1986).
2. C. A. Forster, S. D. Sampson, L. M. Chiappe, D. W. Krause, *Science* **279**, 1915 (1998).
3. P. C. Sereno, *Science* **284**, 2137 (1999).
4. P. J. Makovicky, S. Apesteguía, F. L. Agnolin, *Nature* **437**, 1007 (2005).
5. M. A. Norell *et al.*, *Am. Mus. Novit.* **3545**, 1 (2006).
6. X. Xu, Z. Zhou, X.-l. Wang, *Nature* **408**, 705 (2000).
7. X. Xu, M. A. Norell, X.-l. Wang, P. J. Makovicky, X.-C. Wu, *Nature* **415**, 780 (2002).
8. M. A. Norell, X. Xu, *Nature* **431**, 838 (2004).
9. Z. Kielan-Jaworowska, R. Barsbold, *Palaeontol. Pol.* **27**, 5 (1972).
10. D. Dashzeveg *et al.*, *Am. Mus. Novit.* **3498**, 1 (2005).
11. M. A. Norell, P. J. Makovicky, *Am. Mus. Novit.* **3282**, 1 (1999).
12. A. Elzanowski, P. Wellnhofer, *Am. J. Sci.* **293**, 235 (1993).
13. P. J. Makovicky, M. A. Norell, in *The Dinosauria,* D. B. Weishampel, P. Dodson, H. Osmólska, Eds. (Univ. of California Press, Berkeley, CA, ed. 2, 2004), pp. 184–195.
14. P. J. Makovicky, M. A. Norell, J. M. Clark, T. Rowe, *Am. Mus. Novit.* **3402**, 1 (2003).
15. M. A. Norell, J. A. Clarke, *Nature* **409**, 181 (2001).
16. J. A. Clarke, Z. Zhou, F. Zhang, *J. Anat.* **208**, 287 (2006).
17. Materials and methods are available as supporting material on *Science* Online.
18. A. H. Turner, S. H. Hwang, M. A. Norell, *Am. Mus. Novit.* **3557**, 1 (2007).
19. F. E. Novas, D. Pol, *Nature* **433**, 858 (2005).
20. Q. Ji *et al.*, *Geol. Bull. China* **24**, 197 (2005).
21. M. T. Carrano, in *Amniote Paleobiology: Perspectives on the Evolution of Mammals, Birds, and Reptiles*, M. T. Carrano, T. J. Gaudin, R. W. Blob, J. R. Wible, Eds. (Univ. of Chicago Press, Chicago, 2006), pp. 225–268.
22. Z. Zhou, *Naturwissenschaften* **91**, 455 (2004).
23. E. Buffetaut *et al.*, *Naturwissenschaften* **92**, 477 (2005).
24. K. Padian, A. J. de Ricqlés, J. R. Horner, *Nature* **412**, 405 (2001).
25. X. Xu, Q. Tan, X. Zhao, L. Tan, *Nature* **447**, 844 (2007).

26. We thank the field crew of the 1993 field season for their work; X. Xu, Z. Zhou, C. Forster, and D. Krause for specimen access; P. Makovicky, N. Smith, J. Conrad, A. Balanoff, G. Bever, R. Irmis, and S. Nesbitt for discussions; M. Ellison for photographs; and B. Amaral, A. Davidson, and A. Balcarcel for preparation. Support was provided by NSF through a Doctoral Dissertation Improvement Grant (DEB 0608003, presented to A.H.T. and M.A.N.); grant ATOL 0228693 (presented to M.A.N.); the Program in Geoscience, Division of Earth Sciences (grant EAR 0207744, presented to G.M.E. and M.A.N.); and the Division of Biological Infrastructure, Program in Biological Databases and Information (grant DBI 0446224, presented to G.M.E.). Additional support was provided to A.H.T. by the American Museum of Natural History and Columbia University.

Supporting Online Material

www.sciencemag.org/cgi/content/full/317/5843/1378/DC1
SOM Text
Figs. S1 to S5
References

20 April 2007; accepted 30 July 2007
10.1126/science.1144066

20th-Century Industrial Black Carbon Emissions Altered Arctic Climate Forcing

Joseph R. McConnell,[1]* Ross Edwards,[1] Gregory L. Kok,[2] Mark G. Flanner,[3] Charles S. Zender,[3] Eric S. Saltzman,[3] J. Ryan Banta,[1] Daniel R. Pasteris,[1] Megan M. Carter,[4] Jonathan D. W. Kahl[4]

Black carbon (BC) from biomass and fossil fuel combustion alters chemical and physical properties of the atmosphere and snow albedo, yet little is known about its emission or deposition histories. Measurements of BC, vanillic acid, and non–sea-salt sulfur in ice cores indicate that sources and concentrations of BC in Greenland precipitation varied greatly since 1788 as a result of boreal forest fires and industrial activities. Beginning about 1850, industrial emissions resulted in a sevenfold increase in ice-core BC concentrations, with most change occurring in winter. BC concentrations after about 1951 were lower but increasing. At its maximum from 1906 to 1910, estimated surface climate forcing in early summer from BC in Arctic snow was about 3 watts per square meter, which is eight times the typical preindustrial forcing value.

Emissions of black carbon (BC) particles result from incomplete combustion during the burning of biomass and fossil fuels (*1*). In the atmosphere, the absorption of sunlight by BC contributes to global warming and alters cloud-formation processes (*2*). Arctic climate is especially vulnerable to BC deposition because of its impact on the albedo of snow, glaciers, and sea ice—accelerating melting and increasing sensitivity to warming (*3*). Despite its importance, little is known about past natural or anthropogenic emissions of BC and its deposition. Glaciers and ice sheets contain a historical record of atmospheric deposition of aerosol-borne chemicals derived from natural and anthropogenic burning. We used measurements

of central Greenland ice cores to assess the origin and climate forcing of BC in snow during the past 215 years. Vanillic acid (VA) and non–sea-salt sulfur (nss-S) were used as indicators of forest fires and industrial pollution, respectively.

We used continuous melter analyses of BC, VA, a wide range of trace elements, and hydrogen peroxide (*4*–*6*). BC was analyzed with a laser-based atmospheric analyzer and VA with electrospray triple-quadrupole mass spectrometry (*6*). Measurements were made on an ice core collected in 2003 from a high-snowfall region of west central Greenland, the D4 site (*6*). Using the known midwinter minimum of hydrogen peroxide concentration in Greenland snow (*7*) and assuming uniform snowfall rate within each year (*6*), we determined monthly and annual BC concentration in Greenland from 1788 through 2002 (Fig. 1A).

BC concentrations varied significantly during the past 215 years and were highly seasonal, particularly during the period before industrialization, beginning in the mid-1800s (Fig. 1A) (*6*). Average preindustrial annual BC concentration was 1.7 ng g^{-1}, with generally consistent low winter (defined as December through May) concentrations averaging 1.3 ng g^{-1} and highly variable summer (defined as June through November) concentrations averaging 2.0 ng g^{-1}. After 1850, annual BC concentrations began a gradual rise, followed by a rapid increase in ~1888. Annual average concentrations reached a peak of >12.5 ng g^{-1} in 1908 before beginning a general, although erratic, decline through the late 1940s followed by a sharp drop in 1952. Maximum winter BC concentration peaked in 1908 at more than 20 ng g^{-1}, with an average wintertime concentration of ~13 ng g^{-1} during the highest 5-year period (1906 through 1910), which is about 10 times the mean winter concentration of 1.3 ng g^{-1} before 1850. During the period from 1851 to 1951, annual average concentrations were 4.0 ng g^{-1}, with mean winter and summer concentrations of 4.1 and 3.9 ng g^{-1}, respectively. From 1952 to 2002, average annual concentrations were 2.3 ng g^{-1} and were characterized by high year-to-year variability in summer and a gradual decline in winter BC concentrations through the end of the century (Fig. 1B). Although highly variable with season and year, monthly BC concentrations during the late 20th century (Fig. 1A) ranged from <1 ng g^{-1} to >10 ng g^{-1} and are in general agreement with published measurements of BC in Greenland snow (*8*–*11*).

Although changes in BC measured in the D4 ice core are substantial, it is unclear from a single ice-core record whether the observed changes are representative of central Greenland or the larger Arctic region. As a first step in determining this, we made similar, although discontinuous, measurements from a second ice core collected at the D5 site, ~350 km to the south of D4 (*6*). Changes in BC during the past two centuries (Fig. 1B) were similar at both sites (*6*), suggesting that many of the large summer increases associated with boreal forest fires before industrialization, and the marked increases in winter and spring BC during and after industrialization, were regional and represent central Greenland and possibly much of the Arctic, including the seasonally snow-covered regions of northern and eastern Canada and sea-ice–covered areas of the North Atlantic.

To investigate BC sources in the Greenland records, we used ice-core measurements (*6*) of the conifer-specific forest fire indicator VA (*12*, *13*) and measurements of nss-S as an indicator of industrial emissions (mostly from fossil fuel combustion) (*6*, *14*).

Comparisons of annual average BC and VA concentrations suggest that conifer combustion was the major source of BC in Greenland before 1850 (Fig. 2A) and a significant source during summer throughout the 215-year record. Before 1850, variations in BC concentrations closely matched changes in VA concentrations. Correlations between annual, winter, and summer concentrations of VA and BC were 0.87, 0.72, and 0.87 ($P < 0.0001$), respectively. During the period from 1850 to 1951, correspondence between VA and BC concentration dropped dramatically, particularly in winter. Although correlations between annual and summer average concentrations remained significant (annual: $r = 0.56$, $P < 0.0001$; summer: $r = 0.34$, $P < 0.0005$), winter concentrations showed no covariance. From 1951 to 2002, winter concentrations also were uncorrelated, whereas the correlation in summer concentrations remained at 0.44 ($P < 0.0008$).

Air-mass back-trajectory modeling suggests that the eastern and northern United States and Canada are likely source regions of BC measured at the D4 ice-core site (*6*). We used the National Oceanic and Atmospheric Administration Climate Monitoring and Diagnostics Laboratory atmospheric trajectory model (*15*), driven by velocity fields from the ERA-40 reanalysis for 1958 through 2002 (*16*). Modeling suggests that most BC is wet-deposited and has an atmospheric lifetime of ~3 days (*11*), so we used 3-day trajectories corresponding only to major snowfall events. Given the model results and close correspondence between summer BC and VA, the likely source of BC from biomass burning is the conifer-rich boreal forest of eastern North America.

Northern Hemisphere industrial emissions of sulfur dioxide began in the mid-19th century with widespread burning of coal (*17*), and the ice-core record clearly reflects this (Fig. 2B). Before 1850, nss-S concentrations were generally low and primarily attributed to biogenic emissions (*14*), although the entire ice-core record is punctuated with very large, short-lived increases in nss-S resulting from fallout from well-known explosive volcanic eruptions. Long-term increases in nss-S began soon after 1850, accelerated sharply during the late 19th century, declined slowly from ~1910 to the late 1930s, and then increased strongly again through the early 1970s. In the early 1970s, implementation of the Clean Air Act lowered U.S. sulfur emissions (other countries also began regulating emissions), resulting in a peak in nss-S in the D4 ice-core record in ~1970 followed by a slow decline until ~1992 and a sharp drop almost to preindustrial levels by 2002.

Before 1850, when correlations between BC and VA were high, concentrations of nss-S were not correlated to either BC or VA, suggesting that forest fires were not a significant source of

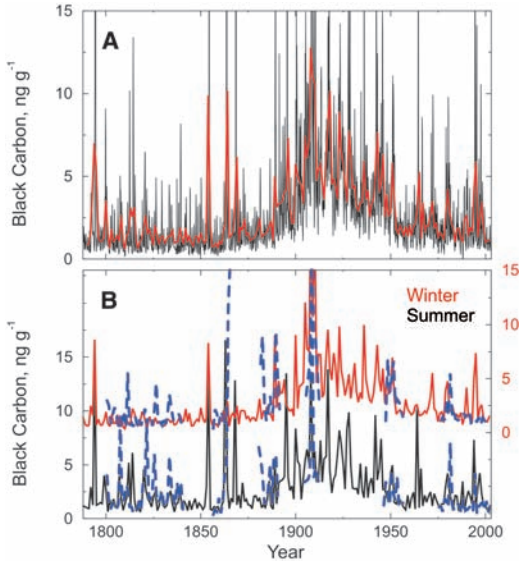

Fig. 1. (**A**) Monthly (black) and annual (red) BC concentrations from 1788 through 2002 measured in the Greenland D4 ice core. (**B**) Winter and summer BC concentrations show that long-term changes in BC were greater in winter (red) than in summer (black) during the late 19th and early 20th centuries. Winter and summer BC concentrations measured in the D5 ice core (*6*), located ~350 km south of the D4 site (blue dashed trace), indicate that observed BC changes were at least regional in extent. The maximum monthly BC value of 58.8 ng g^{-1} occurred in summer 1854.

[1]Desert Research Institute, Nevada System of Higher Education, Reno, NV 89512, USA. [2]Droplet Measurement Technologies, Boulder, CO 80301, USA. [3]Department of Earth System Science, University of California, Irvine, CA 92697, USA. [4]Department of Mathematical Sciences, University of Wisconsin–Milwaukee, Milwaukee, WI 53201, USA.

*To whom correspondence should be addressed. E-mail: Joe.McConnell@dri.edu

atmospheric sulfur. After 1850, highly correlated increases ($P < 0.0001$) in BC and nss-S concentrations indicate that industrial emissions became the primary source of BC. Correlations between annual, winter, and summer average BC and nss-S concentrations from 1850 to 1951 were 0.67, 0.74, and 0.59, respectively. Comparisons of BC and nss-S concentrations during winter, when forest fire–derived BC was at a minimum, indicate that for every ton of pollution nss-S deposited in winter precipitation from 1850 to 1951, an average of ~0.3 ton of BC was deposited concurrently (*6*). After 1951, the positive correlation between nss-S and BC concentration decreased dramatically. Despite large increases in industrial SO_2 emissions (*17*) and nss-S concentrations in the ice-core record, BC concentrations in the ice remained low. Some correlation between nss-S and BC concentrations, however, was still evident (annual: $r = 0.30$, $P < 0.02$), albeit substantially less significant than during the period of high BC concentrations.

Although not validated because of the paucity of historical 20th-century BC measurements before this study, estimates of industrial BC emissions have been made on the basis of records of fossil fuel combustion (*18*, *19*). Such estimates were determined using fuel- and technology-dependent emissions factors that relate BC emissions to fuel combusted. Technological changes through time, however, mean that emissions factors are highly uncertain. Of the estimates of 20th-century BC emissions reported by (*18*), our measurements of BC agree most closely with those from the United States. In particular, estimates of U.S. emissions show a rapid increase in the late 18th century, a leveling off and decline in the early 20th century, a sharp drop in the early 1950s, and a slow decline to the end of the century—very similar to the ice-core measurements. Some models suggest that a large fraction of Arctic pollutants originates in south Asia (*3*). From results of air-mass back-trajectory modeling (*6*), as well as comparisons of ice-core measurements of BC and lead (*20*) with estimated BC and lead atmospheric industrial emissions, we conclude that most of the industrial BC deposited in central Greenland precipitation probably came from North American emissions, at least during the period of high BC concentrations from 1850 to 1951. Since 1951, the positive BC trend in the core record attributed to industrial emissions (Fig. 2A) suggests that Asia may be the primary source today, which is consistent with other work (*3*).

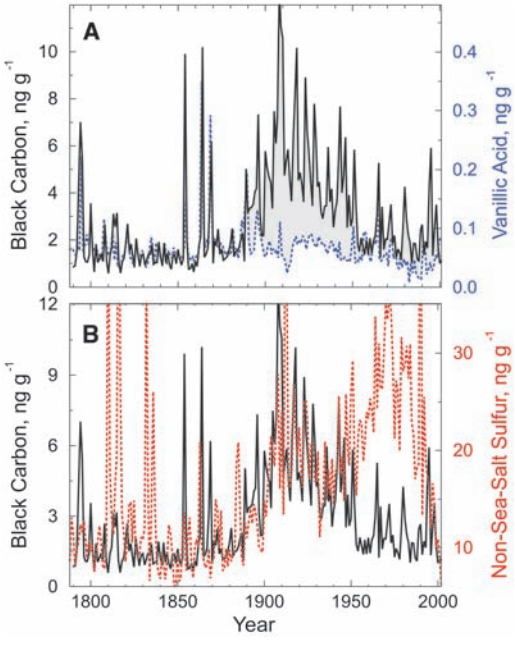

Fig. 2. (**A**) Annual average concentrations of BC and VA. The gray shaded region represents the portion of BC attributed to industrial emissions, not boreal forest fires. (**B**) Annual average concentrations of BC and nss-S. Large short-lived increases in nss-S result from explosive volcanism (such as Tambora, 1816; Krakatoa, 1883; and Katmai, 1912).

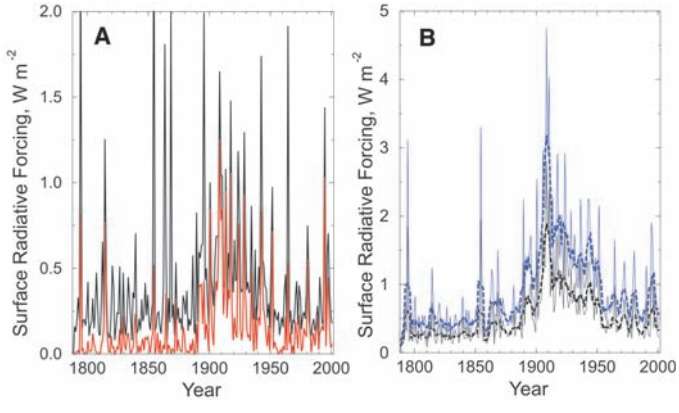

Fig. 3. (**A**) Surface radiative forcing from BC in snow during early summer (June and July) at the permanently snow-covered D4 ice core site. Forcing was modeled using SNICAR and monthly averaged total (black) and industrial (red) BC concentrations. (**B**) Estimated surface radiative forcing for a seasonal snow cover derived using mean winter BC concentration measured in the core and early summer solar forcing conditions (black). Average early summer surface forcing was extrapolated throughout the Arctic region (blue). The dashed lines show 5-year running means. Modeling of radiative forcing at the ice core site was for dry snow conditions because no surface melt occurs at D4. Although poorly known, redistribution of BC in a melting snow pack (*22*) may influence the impact of BC on forcing.

This monthly resolved record of BC in Arctic precipitation allows quantitative estimation of the impacts on climate forcing of BC in snow from both forest fires and fossil fuel burning during recent centuries. We used the Snow, Ice, and Aerosol Radiative (SNICAR) model (*11*), assuming an ice-grain effective radius of 100 μm and mass distributions measured in the ice core (a median particle mass of 1.82 fg and a geometric log-normal distribution width of 2.64) (*6*).

Because of large seasonal changes in incoming radiation at high latitudes and sometimes large seasonal changes in BC concentration in the ice-core record, radiative forcing from BC in snow in central Greenland is highly seasonal (*6*) and increased markedly during the late 19th and early 20th centuries as a result of industrial pollution. Monthly averaged surface forcing (i.e., BC-induced heating) during the peak early summer period (June and July) was ~0.28 W m^{-2}, with a median early summer forcing of ~0.20 W m^{-2} before 1850, ~0.38 W m^{-2} from 1850 to 1951, and ~0.22 W m^{-2} after 1951. Forcing during the dark winter months was negligible. During the peak 5-year period from 1906 to 1910, forcing at the D4 ice-core site from BC in snow was 1.02 W m^{-2}, a fivefold increase from preindustrial conditions, with ~0.76 W m^{-2} attributed to industrial pollution BC (Fig. 3A).

Although enhanced radiative forcing from BC in snow results in warming and possibly summer melting on the permanently snow-covered Greenland ice sheet, potential impacts on seasonal snow covers are larger because additional warming leads to earlier exposure of underlying low-albedo rock, soil, vegetation, and sea ice (*19*). Surface heating in seasonally snow-covered regions is primarily influenced by BC deposited during the snow accumulation period (December through May). Thus, early summer surface radiative forcing for a seasonally snow-covered site can be estimated using average BC concentration from December through July, measured in the ice core, and solar forcing conditions during the subsequent early summer

(Fig. 3B). In simulations with these conditions, the radiative impact of industrial BC emissions is substantially greater because winter concentrations increase more than summer concentrations as a result of industrialization.

To estimate the impact of changes in BC measured in ice cores throughout the Arctic region during the past 215 years, we used global model simulations of 1998 and 2001 radiative forcing from BC in snow to extrapolate model results at the ice-core site (*11*). The simulated average surface forcing of anthropogenic BC throughout the region from 60°N to 90°N was 1.7 times that at the ice-core site in Greenland. Assuming that this ratio has been approximately constant in time, we scaled monthly average surface forcing for the seasonal snow-cover simulation to approximate changes in average Arctic surface forcing during the same period (Fig. 3B). Although they are in agreement with these results in central Greenland, 1983–1984 spot measurements of BC indicated an Arctic/Greenland value of about 10 (*21*), suggesting that the impact from industrial BC emissions across the Arctic may have been significantly larger.

Pronounced increases in BC concentration in snow observed in the Greenland ice cores extrapolate to a marked impact on early summer climate forcing throughout the Arctic during and after industrialization, with changes largely attributed to winter industrial BC emissions (Fig. 3B). The median in estimated surface forcing in early summer throughout the Arctic was 0.42 W m^{-2} before 1850, 1.13 W m^{-2} during the period from 1850 to 1951, and 0.59 W m^{-2} after 1951. During the 5-year period of maximum industrial BC emissions from 1906 to 1910, estimated surface forcing in the Arctic was 3.2 W m^{-2}, which is about eight times the typical early summer forcing before industrialization.

References and Notes

1. Intergovernmental Panel on Climate Change, *IPCC Third Assessment Report, Climate Change 2001: The Scientific Basis* (Cambridge Univ. Press, Cambridge, 2001).
2. M. Z. Jacobson, *Nature* **409**, 695 (2001).
3. D. Koch, J. Hansen, *J. Geophys. Res.* **110**, 10.1029/2004JD005296 (2005).
4. J. R. McConnell, G. W. Lamorey, S. W. Lambert, K. C. Taylor, *Environ. Sci. Technol.* **36**, 7 (2002).
5. J. R. McConnell, A. J. Aristarain, J. R. Banta, P. R. Edwards, J. C. Simões, *Proc. Natl. Acad. Sci. U.S.A.* **104**, 5743 (2007).
6. Materials and methods are available as supporting material on *Science* Online.
7. J. R. McConnell, R. C. Bales, J. R. Winterle, H. Kuhns, C. R. Stearns, *J. Geophys. Res.* **102**, 26809 (1997).
8. G. Holdsworth *et al.*, *J. Geophys. Res.* **101**, 23317 (1996).
9. P. Chylek, B. Johnson, H. Wu, *Geophys. Res. Lett.* **19**, 1951 (1992).
10. P. Chylek, B. Johnson, P. A. Damiano, K. C. Taylor, P. Clement, *Geophys. Res. Lett.* **22**, 89 (1995).
11. M. G. Flanner, C. S. Zender, J. T. Randerson, P. J. Rasch, *J. Geophys. Res.* **112**, 10.1029/2006JD008003 (2007).
12. B. R. T. Simoneit, *Appl. Geochem.* **17**, 129 (2002).
13. P. M. Fine, G. R. Cass, B. R. T. Simoneit, *Environ. Eng. Sci.* **21**, 387 (2004).
14. N. Patris *et al.*, *J. Geophys. Res.* **107**, 10.1029/2001JD000672 (2002).
15. J. M. Harris, J. D. W. Kahl, *J. Geophys. Res.* **99**, 25845 (1994).
16. S. M. Uppala *et al.*, *Q. J. R. Meteorol. Soc.* **131**, 2961 (2005).
17. S. J. Smith, H. Pitcher, T. M. L. Wigley, *Global Planet. Change* **29**, 99 (2001).
18. T. Novakov *et al.*, *Geophys. Res. Lett.* **30**, 10.1029/2002GL016345 (2003).
19. J. Hansen, L. Nazarenko, *Proc. Natl. Acad. Sci. U.S.A.* **101**, 423 (2004).
20. J. R. McConnell, G. W. Lamorey, M. A. Hutterli, *Geophys. Res. Lett.* **29**, 2130 (2002).
21. A. D. Clarke, K. J. Noone, *Atmos. Environ.* **19**, 2045 (1985).
22. H. Conway, A. Gades, C. F. Raymond, *Water Resour. Res.* **32**, 1713 (1996).

23. Collection and analysis of the Greenland ice cores were supported by NSF Arctic Natural Sciences (J.R.M, R.E, J.R.B, and D.R.P), including development of the analytical method for VA (J.R.M. and E.S.S). Development of the BC analytical method was supported by NSF Arctic Natural Sciences, NSF Earth Sciences: Instrumentation and Facilities, and the Desert Research Institute (R.E., G.L.K, and J.R.M.); and development of the Single Particle Soot Photometer 2 was supported by a Small Business Innovation Research grant to Droplet Measurement Technologies by the Office of Naval Research. Atmospheric trajectory modeling was supported by NASA's Cryospheric Processes Program (J.R.M., J.D.W.K, and M.M.C). Simulations were supported by a NASA Earth System Science Fellowship and NSF Atmospheric Sciences (M.G.F. and C.S.Z.). R. Kreidberg provided help in editing the manuscript.

Supporting Online Material

www.sciencemag.org/cgi/content/full/1144856/DC1
Materials and Methods
Figs. S1 to S4
References

9 May 2007; accepted 31 July 2007
Published online 9 August 2007;
10.1126/science.1144856
Include this information when citing this paper.

Saturn's Gravitational Field, Internal Rotation, and Interior Structure

John D. Anderson[1]* and Gerald Schubert[2]

Saturn's internal rotation period is unknown, though it must be less than 10 hours, 39 minutes, and 22 seconds, as derived from magnetic field plus kilometric radiation data. By using the Cassini spacecraft's gravitational data, along with Pioneer and Voyager radio occultation and wind data, we obtain a rotation period of 10 hours, 32 minutes, and 35 ± 13 seconds. This more rapid spin implies slower equatorial wind speeds on Saturn than previously assumed, and the winds at higher latitudes flow both east and west, as on Jupiter. Our related Saturn interior model has a molecular-to-metallic hydrogen transition about halfway to the planet's center.

Because of its rapid rotation, Saturn is the most oblate planet in the solar system. The flattening of the planet can be seen even through a small telescope. However, the planet's internal rotation rate is not reflected in the measured periodicities in magnetic field data and Saturn kilometric radiation (SKR) data (*1*). Periodic signals coherent in period, amplitude, and phase over several months, including the Cassini rotation period of 10 hours, 47 min, 6 s (*2*), do not reflect the rotation of the deep interior but rather are based on a slippage of Saturn's magnetosphere relative to the interior, possibly due to a centrifugally driven instability in Saturn's plasma disk (*1*, *3*). For the purposes of obtaining a reference geoid and interior density distribution, both of which are dependent on Saturn's deep rotation rate, we analyze the available gravitational data (*4*) and radio occultation and wind data (*5*) with an approach free of any tight a priori constraints on Saturn's rotation period.

[1]121 South Wilson Avenue, Pasadena, CA 91106–3017, USA. [2]Department of Earth and Space Sciences and Institute of Geophysics and Planetary Physics, University of California, Los Angeles, CA 90095–1567, USA.

*To whom correspondence should be addressed. E-mail: jdandy@earthlink.net

The gravitational data reflect Saturn's interior density distribution and internal rotation rate, whereas the radio occultation and wind data reflect dynamical effects on the shape of a surface of constant pressure: the 100-mbar isosurface in Saturn's atmosphere. By finding a mean geoid (a static surface of equal gravitational potential energy) that both matches the gravitational data and minimizes the wind-induced dynamic heights of the 100-mbar isosurface with respect to the mean or reference geoid, we average out the dynamical effects on the atmosphere and obtain a static oblate Saturn model. We claim that this model, which minimizes the energy needed to drive the atmospheric winds, is a good approximation to the true physical state of Saturn below its atmosphere. The more rapid spin we find to be associated with the reference geoid affects atmospheric dynamics. The eastern wind speeds on the equator are reduced, corresponding to a reduction in the equatorial bulge from 122 to 10 km.

The history of the figures of celestial bodies in uniform rotation is a rich one and of considerable interest in itself [e.g., see chapter 1 in both (*6*) and (*7*)]. An important result from Newtonian mechanics, which is sufficient for the description of the shape of planetary bodies and stars, is that the external gravitational potential